SANDT-PRO: SEDIMENT TRANSPORT MEASUREMENTS UNDER IRREGULAR AND BREAKING WAVES

Jan S. Ribberink[1] , Dominic A. van der A[2], Joep van der Zanden[3], Tom O'Donoghue[4], David Hurther[5], Iván Cáceres[6], Peter D. Thorne[7]

First results are presented of a measurement campaign done in the large-scale Barcelona CIEM wave flume from October 2013 to January 2014. The aim of the experiments was to improve our understanding of sediment transport processes in the near-shore region. In particular, we focused on the effects of (1) wave breaking and (2) wave irregularity on net sediment transport rates and sediment transport processes. High-resolution measurements were obtained using advanced instrumentation, deployed from a custom-built measuring frame that could be horizontally and vertically positioned. These instruments provide detailed insights in the vertical distributions of sediment fluxes. Preliminary results from the breaking-wave experiments show an onshore transport of sediment prior to breaking, likely to be dominated by wave-nonlinearity effects, and an offshore sediment flux shoreward of breaking, where the sediment fluxes are undertow-dominated.

Keywords: sediment dynamics, sediment transport, breaking waves, surf zone, irregular waves, wave flume experiments, sheet flow

INTRODUCTION

The complex interactions between hydrodynamics and sediment transport processes in the near-shore coastal region are not yet understood at a level of detail required for accurate model predictions of morphodynamics (see e.g.Van Rijn et al., 2013). This holds in particular for the effects of wave irregularity and wave breaking, and is primarily caused by a lack of detailed experimental hydrodynamic and sediment flux data, especially near the sea bed and in controlled large-scale conditions. Previous experiments were often carried out in small-scale wave flumes (e.g. Deigaard et al., 1986; Butt et al., 2004), had their focus on hydrodynamics and suspended sediment higher in the water column (e.g. Roelvink and Reniers, 1995; Maddux et al., 2006), or focused wholly on beach profile changes and total net transport rates (e.g. Van Rijn, 2009; Baldock et al., 2011).

Our research aims are i) to uncover further the physical processes that drive sand transport under different types of regular breaking and irregular non-breaking waves, and ii) to generate a high-quality dataset of detailed flow, sediment concentration and sediment flux measurements in controlled large-scale conditions. This is achieved through a new series of mobile-bed wave flume experiments in the large CIEM flume of UPC in Barcelona involving medium to large-scale waves, and by using advanced measuring instruments, which became available recently (CCM[+], HR-ACVP). Compared to earlier experiments, the new experiments yield greater detail and insights into the bottom boundary layer processes and near-bed sediment transport fluxes.

Between October 2013 and January 2014 two types of experiment were conducted: i) Experiments involving regular breaking (RB) waves, focusing on the effects of wave breaking on the near-bed sediment dynamics in the wave bottom boundary layer (WBBL) and on suspended sediment advection processes; ii) Experiments with irregular non-breaking (INB) waves, focusing on turbulence and sediment pumping under wave groups and the effect of wave sequence on the wave-related sediment flux in the suspension layer.

EXPERIMENTAL SET-UP

Wave flume, sand bed and measuring instrumentation

The experiments were carried out in the 100 m long CIEM flume using water depths of 2.55 m and 2.65 m in front of the wave paddle. The initial sand bed consisted of an offshore linear slope (1:10

during most experiments), followed by a 20 m long horizontal test section with a sand bed height of 1.35 m. At the shore side the sand bed is enclosed by a fixed beach, consisting of sand covered with a layer of geotextile and concrete blocks, which was constructed in a parabolic shape to dissipate the remaining wave energy as much as possible (Figure 1). The sand bed material consists of medium-grained sand with a D_{50} of 0.25 mm.
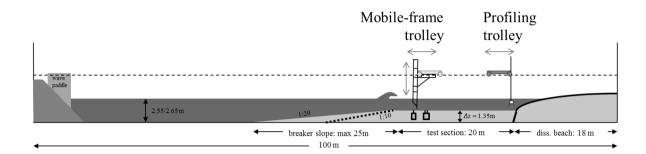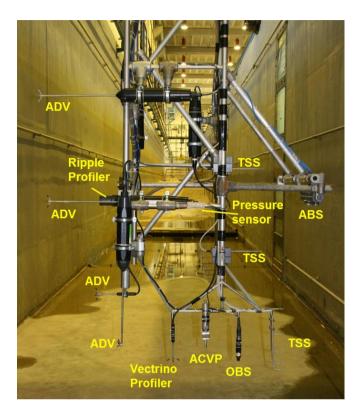

Figure 1. CIEM wave flume with sand bed and fixed dissipative beach; trolley with instrumented frame (left), bed profiling trolley (right) and 2 CCM tanks in the bed .

Detailed measurements of sediment concentrations and flow velocities were carried out using a vertical array of instruments, deployed from a mobile measuring frame that was custom-built at the University of Twente. This frame consists of 30mm stainless steel tubing, mounted to the bottom of a horizontally-mobile carriage located above the flume (Figure 1). The entire frame can be vertically positioned over 1.4 m with O(mm) accuracy using a spindle. The frame was designed such that it was as stiff as possible, while at the same time flow perturbations were tried to be minimized.

A range of instruments to measure sediment concentrations, flow velocities, bed- and water surface elevation was deployed from the frame (Figure 2). In the near-bed layer (5 - 10 cm above the bed) water-sediment mixture velocities (2DV components) and sediment concentrations were sampled simultaneously with a vertical resolution of 1.5 mm using a new High-Resolution Acoustic Concentration and Velocity Profiler (based on ACVP-technology described in Hurther et al., 2011 and Hurther and Thorne, 2011; see Figure 2). Very close to and inside the bed in the sheet flow layer (thickness of order 1 cm) new Conductivity Concentration Measuring sensors (CCM[+], see Van der Zanden et al., 2013 and Figure 2) were deployed from two tanks buried in the sand bed. Apart from measuring sediment concentrations and particle velocities, the new CCM[+] probes are able to track and follow the bed-level evolution during the experiment and keep the CCM probe-heads at all times inside the sheet flow layer, also during severe sedimentation or erosion. Above each CCM[+] tank, a separate fixed frame was deployed from the wall with each frame containing an Acoustic Doppler Velocimeter (ADV) and an additional HR-ACVP system.

In addition a range of other state-of- the-art instrumentation was deployed from the mobile frame, partly to be used as reference for the near-bed measurements (3D-Nortek Vectrino Profiler, Optical Backscatter System OBS) or to measure velocities and concentrations higher in the vertical (ADVs, OBSs and an AQUAscat Acoustic Backscatter Sensor ABS operating with 4 acoustic sensors). The concentration measurements are calibrated and verified with suction measurements of suspended sediment, obtained with a 7-nozzle Transverse Suction System (TSS). The suction samples were sieved and dry-weighted to yield time-averaged concentrations and, later, sampled for laser-diffraction-based grain-size analysis. Ripple scans were made using a 2D acoustic Sand Ripple Profiler (SRP). In addition to pre- and post-run SRP scans for each run, continuous scans during wave action were made for a selected few runs. A pore-pressure transducer was deployed from the frame to obtain the local water surface elevation.

Along the flume water surface elevation was measured with 13 resistive wave gauges and, near the wave breaking location, with 9 pore pressure transducers located at 1 m intervals. Total net transport rates are obtained from mass conservation using pre- and post-test bed profiles measured with echo sounders, deployed from a second horizontally-mobile carriage on top of the flume (see Figure 1).
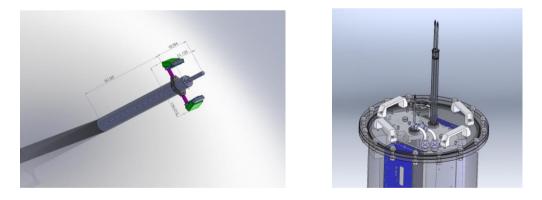
Figure 2. Mobile trolley frame with instrumentation (upper plot), High-Resolution Acoustic Concentration and Velocity Profiler HR-ACVP (left below) and Conductivity Concentration Meters with bed-level tracking CCM+ (right below).

REGULAR BREAKING WAVES (RB)

Experimental conditions and measuring procedures

The RB experiments were carried out for 2 initial bed-slope configurations resulting in 2 different breaking wave conditions: a 1:10 slope which resulted in a plunging breaker condition (RB1) and 1:20 slope which resulted in a 'spilling to plunging' condition (RB2). The water depth and waves were tuned in such a way that initial wave breaking started at the offshore end of the horizontal sand bed (see Table 1). While a breaker bar/trough system slowly developed in the (initially horizontal) test section, sand transport process measurements were carried out during successive experimental runs at various cross-shore positions along the sand bed, covering the shoaling area as well as the breaker and surf zone

area. Typical run durations varied between 15-30 min, after which the wave-paddle was stopped and the mobile-frame was moved to a different cross-shore location. Between the runs bed profile measurements were made along two different longitudinal transects across the flume. The time interval between two consecutive profile measurements increased with the duration of each experiment since net transport rates decreased once the bar/trough system further developed.

Table 1 Regular Breaking (RB) wave experiments (d_0 = water depth at the wave paddle, d_t = water depth at initial horizontal section, H = target wave height at the wave paddle, T = wave period)								
Case	Slope	d_0 (m)	d_t (m)	H (m)	T (s)	Iribarren	Type	Number of runs
RB1	1:10	2.55	1.20	0.85	4	0.54	Plunging	22
RB2	1:20	2.65	1.30	0.95	4	0.26	Spilling → plunging	26

Evolution of a breaker bar/trough system and bedforms

The continuous breaking of the regular waves promoted the growth of a breaker bar /trough system together with erosion of the upper part of the foreshore slope. The evolution of the bed profile during 365 min of wave action in experiment RB1 is shown in Figure 3. From left to right we can distinguish in the initial profile (red line) the 1:10 bottom slope (x=34 to 48 m), followed by the horizontal test section, and finally the beginning of the fixed parabolic beach (indicated by the bump at x=68.5 m). While growing in height and length the bar migrates a few meters in onshore direction with a slowly decreasing migration velocity. After 365 min the bar has a length of app. 7 m and a height of 60 cm. The bar trough has then a length of app. 5 m and has eroded to a maximum depth of about 25 cm. The foreshore slope erodes over a length of app. 8 m offshore of the bar. Figure 3 also shows the locations where the wave breaking starts (x=54 m, initiation of breaking), app. 2 m before the bar crest, and where the plunging breaker jet hits the water surface (x=57 m), just after the bar crest.

Further observations reveal the presence of large quasi-2D bedforms on the eroding foreshore slope (x<50 m), and a flat bed in the shoaling/outer breaker zone on the offshore slope and around the crest of the bar (x=50 to 58 m). The latter suggests that bedload transport is in the sheet-flow regime here. More onshore in the surf zone, where the wave energy has dropped substantially, a gradual transformation of a flat bed to large quasi-2D crescentic bedforms (x=58 to 61 m) with a height of about 10 cm can be seen, followed by smaller (~5 cm height) 3D ripples in the surf zone (x=61 to 68 m).

Net sand transport pattern

During the development of the bar-trough system the net transport rate shows roughly a pattern of net onshore sand motion in the shoaling area on the offshore side of the bar and net offshore sand motion in the surf zone. Figure 4 shows this transport pattern for experiment RB1 based on a mass conservation calculation using the measured initial and final echo-sounder bed profile (t= 0 – 275 min, bed profiles 8 and 18; the last profile t= 365 min was not used here because it was obtained with a different less accurate measuring technique). The method is applied two times using a zero-transport boundary condition at the offshore as well as the onshore boundary of the sand bed. The two patterns are qualitatively the same but the transport rates slightly differ in absolute magnitude, which is caused by some lateral sand losses in the inner surf zone ($65 < x < 70$ m). The solid green line in Figure 4 (bottom plot) indicates the weighted average of both methods.

The positive onshore net transport in the shoaling area reaches a maximum at the base of the breaker bar (x=51 m), then decreases until zero at approximately the (initial) breaking point (x=55 m). At this location the net transport reverses direction and the decrease continues in the surf zone until a maximum negative transport (offshore-directed) is reached at the beginning of the bar trough (x=57 m). In the bar trough and more onshore net transport rates remain negative but slowly decrease in magnitude.
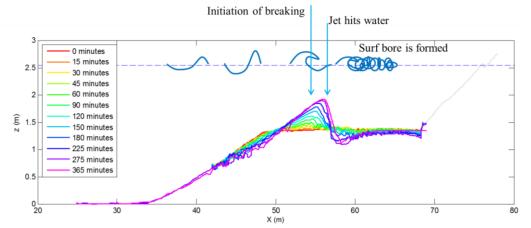
Figure 3. Evolution of the breaker bar: growth and onshore migration of the bar crest goes together with development of the bar trough and erosion of the foreshore (exp. RB1).
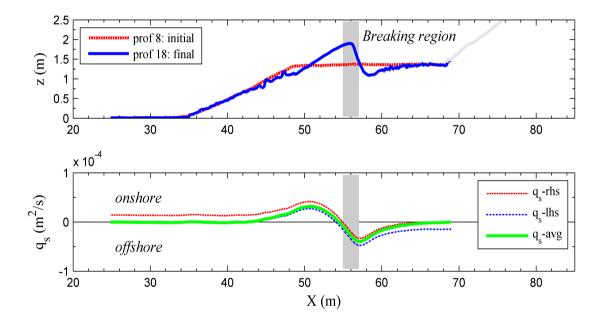

Figure 4. Distribution of the mean net transport rate along the bed based on the measured bed profiles at time t=0 (prof 8: initial bed) and t=275 min (prof 18: final bed used for transport-rate calculations) and conservation of mass (exp. RB1).

Velocities along the bed

Under non-breaking waves it is known that the magnitude and direction of the net sediment transport rate is directly related to the wave–induced flow velocities along the bed above the WBBL (see e.g. Ribberink and Al-Salem, 1994; Van der A et. al, 2013). The velocity pattern along the bed during exp. RB1 is shown in Figure 5 based on the measurements of the lowest ADV (approximately 15 cm above the bed) at 10 locations along the breaker bar and in the inner surf zone. It should be noticed that the measurements are made at different moments during the bar evolution process after some initial

bar development has taken place (t > 90 min). Some locations were revisited 1 or 2 times, leading to 2 or 3 results at these locations. Despite this time-dependency of the bed level a clear and consistent velocity pattern is visible. The measured velocities are split in in a time-averaged component <u> (Fig. 5b) and an oscillatory or wave component u_w (crest and trough amplitudes, Fig. 5d). Moreover, <u^3> of the complete time series (including mean current) is depicted (Fig. 5c).

It is shown that the decaying wave energy caused by wave breaking leads to a considerable reduction of the oscillatory flow near the bed especially in the outer breaker zone (55 < x < 57 m). A considerable velocity skewness ($u_{w,crest} > u_{w,trough}$) is present along the entire bed (Fig. 5d). At the same it can be observed that the mean flow <u>, which is always offshore directed (undertow), shows a strong increase in the outer breaker zone with a maximum in the breaker bar trough (-20 cm/s to -60 cm/s) and decreases slightly again in the inner surf zone (to -40 cm/s). To summarize, in the shoaling zone before wave breaking the oscillatory flow clearly dominates over the mean flow, but in the surf zone the undertow is dominant or is of approximately the same magnitude as the oscillatory velocity amplitude.
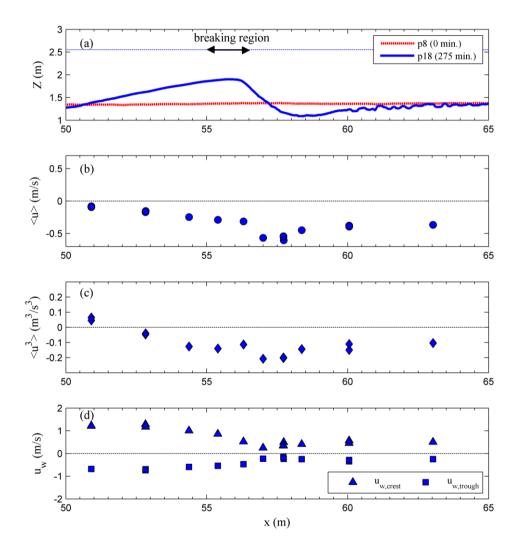

Figure 5 Horizontal mean velocity (b), third-order velocity moment <u^3> of the velocity time series including the mean flow (c) and the orbital velocity maximum/minimum (d) measured along the developing bar and in the inner surf zone (a) at 15 cm above the sand bed using the lowest ADV (exp. RB1).

The velocity moment <u^3> is positive ('onshore') on the offshore slope of the breaker bar (Fig. 5c), but changes sign at approximately x = 52 m. The measured total net transport rates show a similar

sign change (see Figure 4), however this occurs roughly 3 m more onshore at x= 55 m. This qualitative agreement between $<u^3>$ and $<q_s>$ disappears in the inner surf zone. Here $<u^3>$ seems to stabilize to a constant negative magnitude ($\sim - 0.15$ m^3/s^3), while the measured net transport rate drops to zero.

Suspended sediment concentration profiles (time-averaged)

Together with the development of the breaker bar also the intensity of wave-breaking increases and suspended sediment is stirred up to higher levels in the water column. By analyzing the measured time-averaged suspended sediment concentration in the water column $<C(z)>$ together with the undertow $<U>$ an impression can be given of the current-related suspended sediment flux $<C>.<U>$ and its contribution to the total net transport rate. Figure 6 shows a selection of 4 time-averaged sediment concentration profiles, measured with TSS during experiment RB1, between 180 - 365 min after the start of the experiment. This period relates to the final stages of breaker bar development (see also Figure 3). In the shoaling area offshore of the bar crest a gradual increase of suspended sediment load is observed in onshore direction (from x=51.7 to 53.7 m), with still relatively low concentration magnitudes between $0.5 - 0.75$ g/l near the bed ($z = 10$ cm). More onshore in the bar trough ($x = 58.6$ m) the concentrations increase substantially to 1.5 g/l, due to the strong stirring capacity of the breaking wave, while further in the surf zone ($x = 60.9$ m) the concentrations drop again to lower magnitudes. In general, the concentrations also increase strongly near the bed just above or inside the wave bottom boundary layer. It should be noticed that in the sheet flow layer (not shown here) the concentrations are one or two orders of magnitudes larger, reaching magnitudes of 100-500 g/l.

A rough estimate of the offshore directed current-related suspended sediment transport is made for the bar/trough region by multiplying the mean suspended sediment concentration (~ 1.2 g/l) and the mean velocity in this area (~ -0.5 m/s, see Figure 5) with an assumed representative depth of 0.5 m, and dividing by the density of the sediment ($\rho_s = 2.7 \cdot 10^3$ kg/m^3); this leads to a net transport rate of $\sim -1 \cdot 10^{-4}$ m^2/s, which is of the same order of magnitude as the measured net total transport based on the bed-level profiles ($-0.5 \cdot 10^{-4}$ m^2/s, see Figure 4). This clearly indicates that, apart from the near-bed transport in the WBBL, also the suspended sediment load in the water column may contribute importantly to the morphological development of the bar.
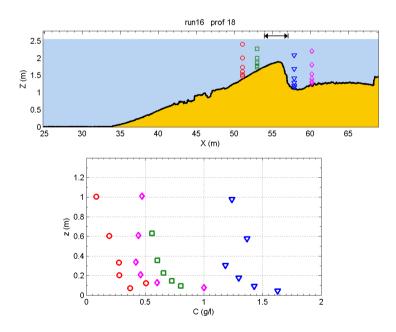

Figure 6. Suspended sediment concentration profiles (time-averaged) in the shoaling region (x=51.7 and 53.7 m) and in the surf zone (x=58.6 and 60.9 m) of experiment RB1 obtained from transverse suction measurements (TSS).

Grain-size sorting

After the RB1 experiment the sand bed was drained carefully and bed samples were taken at 10 positions on the breaker bar and in the surf zone. The grain-size distributions of the samples were measured with a particle size analyzer (Beckman Coulter LS 13 320) and in Figure 7 the resulting D_{50} is shown as a function of the position in the flume. A clear sorting pattern is visible: onshore of the bar crest ($x > 56$ m) the bed became slightly coarser than the original bed material, $D_{50} \sim 290$ μm $> D_{50,original} = 250$ μm. Offshore of the bar crest ($x < 56$ m) on the bar slope the bed material gradually becomes finer in offshore direction, reaching $D_{50} \sim 225$ μm $< D_{50,original} = 250$ μm.

The sorting pattern seems to indicate that in the surf zone especially fine size fractions are stirred up from the bed, leading to some bed coarsening. The relatively fine sediments are then transported in suspension offshore by the mean flow (undertow), which is consistently offshore directed along the whole breaker bar. Along the offshore slope of the bar this fine material reaches the shoaling area, where bed-load dominates and the fine sediments gradually settle to the bed.
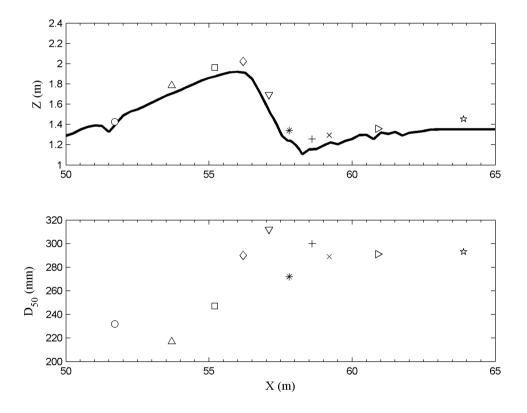

Figure 7. Distribution of the D_{50} of the bed material along the breaker bar and in the surf zone after experiment RB1 (t= 365 min).

Near-bed transport processes: pre and post-breaking (ACVP)

Figure 8 and 9 show phase-average results of the mobile-frame ACVP at 2 selected locations (Figure 8: pre-breaking, $x= 53$ m; Figure 9: post-breaking, $x= 58$ m). Both figures contain phase-averaged velocities, sediment concentrations and fluxes as a function of the scaled intra-wave time t/T and elevation z with respect to the lowest intra-wave bed-level measurement. Note that the sediment concentrations were calculated using default calibration parameters, meaning that the results of the

lower 2 plots are preliminary. In a future stage, the calibration of the ACVP concentrations will be optimized using the measurements of TSS, OBS's, ABS, and net transport rates.

Pre-breaking (Figure 8), free-stream velocities reach a maximum of 1 m/s onshore. This corresponds to a mobility parameter $\psi = u^2/(\Delta gD_{50})$ – with Δ being the relative density of sediment in water (=1.65) – value over 250, corresponding to transport in the sheet-flow regime (e.g. Van Rijn, 2007) which agrees with the observed absence of bedforms in the shoaling zone. The vector fields shown in the middle and lower subplot show typical behavior for near-bed oscillatory flows, including a velocity phase lead near the bed and the velocity overshoot during the wave crest at $z = 2$ cm which indicates the thickness of the WBBL (Jensen *et al.,* 1989). As expected for sheet-flow conditions, high concentration values are found in a thin layer near the bed. The sheet-flow layer is thicker during the crest than during the trough phase of the wave cycle, which leads to a higher flux (Figure 8 lower plot). Hence, the net near-bed transport at this location is positive which agrees with the measured total net transport pattern in Figure 4.
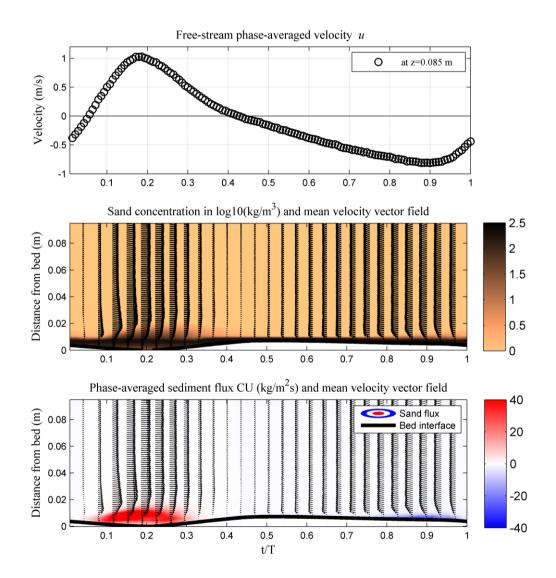

Figure 8. Time-dependent (phase-averaged) velocities, concentrations and sediment fluxes measured with ACVP at *x*= 53 m (shoaling zone). Shown are the 'free-stream' velocity at ~0.08-0.1 m above the bed (upper plot), velocity vector profiles and concentration ([10]logC) contours (middle), velocity vector profiles and sediment flux contours (lower).

Post-breaking (Figure 9), it is clear that the undertow has a dominant effect on near-bed velocities and transport with the free-stream velocity being negative (offshore-directed) during the complete wave cycle. Near-bed sediment concentrations at this location are higher than pre-breaking, which could be a direct effect of wave breaking. Velocity vectors show a strong upward velocity component, since this measurement was taken above the inclined bed at the shoreward side of the breaker bar. The WBBL, which is at this location thicker than on the pre-breaking location, contains again most of the sediment. Within the WBBL, velocities and hence sediment flux are found to be positive for a short instance during the crest phase (between t/T= 0.5 - 0.6). However, the offshore contribution to the local sediment flux is far greater, leading to a net negative flux which is again in agreement with the transport pattern in Figure 4.
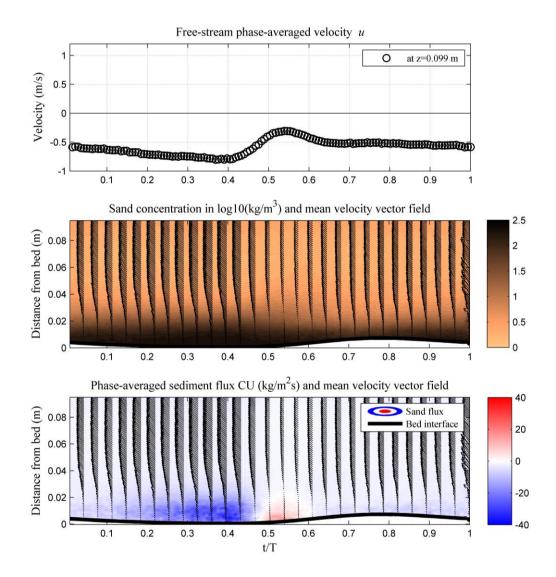

Figure 9. Time-dependent (phase-averaged) ACVP results at x= 58 m (post-breaking). For explanation of subplots, see caption Figure 8.

IIRREGULAR NON-BREAKING WAVES (INB)

Experimental conditions and measuring procedures

The irregular non-breaking wave experiments were carried out with different bichromatic and modulated wave group conditions using the 1:10 offshore bed slope. To realize non-breaking wave

conditions in the test section, the wave height was lower than during the RB experiments and wave breaking only occurred more onshore on the fixed beach. The sand transport process measurements were now concentrated at one cross-shore position in the middle of the horizontal test section.

The wave groups were generated by modulating a regular (short) sine wave time-series (short wave period T) with a (longer) wave (group period $T_g > T$). The rms-wave height was constant for all 5 conditions ($H_{rms} = 0.49$ m), as was the short wave period ($T = 4.4$ s). The group period varied ($T_g = 28.6 – 44$ s) and consequently also the number of short waves in a group varied ($N = 7$-10). For the first three conditions (IGB1, IGB2 and IGB3) the group was generated from two frequency components which differed in frequency such that the group contained an integer amount of waves (N). The other two group conditions (IGM1 and IGM2) were generated by modulating a regular (short) sine wave time-series (short wave period T) with a (longer) wave signal (group period $T_g > T$). A sawtooth shaped modulation signal was used, which enabled the generation of 'waxing' wave groups (slow wave growth and quick wave decay in a group) as well as 'waning' wave groups (quick wave growth and slow wave decay). See Table 2 for an overview of the experimental conditions.

Table 2 Irregular non-breaking wave experiments (wave groups) (T_m = mean wave period, T_g= wave group period, H_α = wave height at the wave paddle (with $\alpha = rms$ = root-mean-square, $\alpha = s$ = significant , $\alpha = max$ = maximum), N = number of waves in the group)								
Case	T_m (s)	H_{rms} (m)	H_s (m)	H_{max} (m)	T_g (s)	N (-)	Type	Total run time (min)
IGB1	4.4	0.49	0.69	0.69	41.8	10	Bichromatic, fully modulated	175
IGB2	4.4	0.49	0.69	0.69	28.6	7	Bichromatic, fully modulated	150
IGB3	4.4	0.49	0.69	0.62	41.8	10	Bichromatic, partial modulated	175
IGM1	4.4	0.49	0.69	0.79	44	10	Waxing, fully modulated	185
IGM2	4.4	0.49	0.69	0.79	44	10	Waning, fully modulated	185

For each condition an experiment consisted of 5 runs each of 50 wave group duration, resulting in a total of 250 wave groups of data per condition. Bed profiles were measured after the first, third and last run.

Suspended sediment

Only a small part of the extensive dataset of velocity and concentration measurements, as collected during the INB experiments, were processed and analyzed until now. Figure 10 shows a first processed result of suspended sediment concentrations measured with ABS for condition IGB1 .

Phase-averaged results over 10 wave groups are shown of concentrations measured with the 2, 3 and 4 MHz ABS transducers (3 lower plots) and water surface elevation measured with the local pressure transducer (upper plot). It is shown that the suspended sediment entrainment and settling processes in the lower 30 cm near the bed occur at the short wave time scale as well as on the wave group time scale. During the short waves two concentration peaks can be observed, which can be related to sediment stirring from the bed during the passage of the wave crest and the wave trough. The largest concentration peaks seem to occur just before the passage of the wave crest. Moreover, sediment concentrations do not drop to zero between the half cycles. The latter indicates that concentration phase lags probably play an important role for the net suspended sediment transport. It should also be noticed

that small 3D bed ripples were present, which can lead to considerable additional phase differences between near-bed velocity and concentrations.

Also on the larger time-scale of the wave group suspension phase-lag effects seem to be present. The wave front of the group shows relatively low concentrations compared to the tail of the group and the 'concentration group' seems to be delayed in phase in comparison with the wave group. This could be an indication for the presence of a sediment 'pumping' effect during the sequence of high waves (see also Vincent and Hanes, 2002) and a settling lag effect during the tail of the wave group.
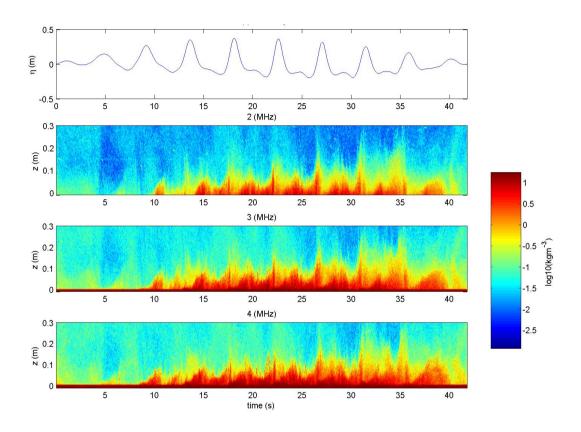

Figure 10.   Time-dependent (phase-averaged) water surface elevation (upper plot) and sediment concentration (^{10}log*C*) contours in the lower part of the water colum (0 < *z* < 30 cm). The concentrations in the three plots are measured with ABS using 2, 3 and 4 MHz transducers.

CONCLUSIONS

A new measuring campaign was carried out in the large-scale Barcelona CIEM wave flume in the collaboration project SandT-Pro. An extensive new dataset of high-resolution flow and sediment measurements was obtained for large-scale breaking waves (RB-experiments) and for irregular grouped waves (INB-experiments) over a mobile sand bed. Much of the data processing and analysis is still to be carried out but some first results and impressions of selected measurements were presented.

The main conclusions can be summarized as follows.
RB-experiments
- The experiments gave good insight in the development of a breaker bar: the building up of the bar occurred with sand coming from two sides: onshore net transport in the shoaling zone before breaking and offshore net transport in surf zone.
- Detailed near-bed measurements, carried out with the new acoustic instrument HR-ACVP, indicate that sediment fluxes in the thin near-bed sheet flow layer (0 – 1 cm above the bed) are much larger than in the suspension layer above; this is observed in the shoaling zone (pre-breaking) but also in the outer breaker zone. The net transport rates in the near-bed layer have

the same direction and are of similar magnitude as the measured total net transport (based on bed level soundings).

- The near-bed onshore transport prior to breaking on the offshore slope of the breaker bar is likely to be dominated by wave-nonlinearity effects. In the surf zone the total net transport is offshore directed and the sediment transport is dominated by a large undertow.

- In the outer breaker zone the breaking-induced suspended sediment mixing is large and concentrations reach relatively high magnitudes also higher in the water column (1 – 100 cm above the bed). This leads to a considerable vertically integrated sediment flux (suspended sediment transport), which is offshore directed and is also of similar magnitude as the measured total net transport at this location.

The INB experiments
- Preliminary analysis of intra-wave suspended sediment concentrations measured with ABS during one of the non-breaking wave group experiments indicates that suspension phase-lag effects occur at the time-scale of the short waves as well at the wave group time scale (sediment pumping).

Upcoming analyses of the new dataset will also include calculations of sediment fluxes using the CCM$^+$ tanks (together with ACVP) and the combination of ABS/ADVs (higher in vertical). Our aim is to obtain a better insight in vertical sediment flux distribution and the transport rates including the various sediment flux/transport components (current, wave, turbulent), and study how these are affected by wave breaking (RB cases) and shape of the wave group (INB cases). Turbulence estimations using the HR-ACVP and Vectrino Profiler will help to understand the observed sediment transport processes.

Moreover, additional experiments in the CIEM wave flume are scheduled in 2014 as part of the joint UK/Dutch collaboration project SINBAD using the same instrument set-up. A first series will involve additional medium-sand runs, with the aim to study the effects of wave breaking on cross-shore flow non-uniformities and sediment transport rates for one breaking-wave condition in more detail. Subsequently, hydrodynamics and boundary-layer flow will be examined in more detail by a series of rigid-bed experiments, in which it will be attempted to use optic measuring instrumentation (PIV, LDA) at this large experimental scale.

The results of the experiments will be used to develop process-based numerical models as well as to improve practical sand transport models (e.g. van Rijn, 2007; SANTOSS model: van der A *et al.*, 2013) that are used in morphodynamic models.

REFERENCES
Baldock, T., Alsina, J., Caceres, I., Vicinanza, D., Contestabile, P., Power, H., A. Sanchez-Arcilla. 2011. Large-scale experiments on beach profile evolution and surf and swash zone sediment transport induced by long waves, wave groups and random waves, *Coast. Eng.* 58 (2), 214–227.

Butt, T., P. Russell, J. Puleo, J. Miles , G. Masselink. 2004. The influence of bore turbulence on sediment transport in the swash and inner surf zones, *Cont. Shelf Res.* 24, p 757 – 771.

Deigaard, R.. J. Fredsoe and I. Broker-Hedegaard. 1986. Suspended sediment in the surf zone. *J. of Waterw., Port, Coast. And Ocean Eng.*, ASCE, Vol. 112, No.1.

Hurther, D., Thorne, P.D., Bricault, M., Lemmin, U. and J.M. Barnoud. 2011. A multi-frequency Acoustic Concentration and Velocity Profiler (ACVP) for boundary layer measurements of fine-scale flow and sediment transport processes, *Coastal Engineering* 58(7): 594-605, doi: 10.1016/j.coastaleng.2011.01.006.

Hurther, D., and P. D. Thorne. 2011. Suspension and near-bed load sediment transport processes above a migrating sand-rippled bed under shoaling waves, *J. Geophys. Res*., 116, C07001, doi:10.1029/2010JC006774.

Jensen, B. L., B. M. Sumer and J. Fredsoe (1989). Turbulent Oscillatory Boundary-Layers at High Reynolds-Numbers. Journal of Fluid Mechanics 206: 265-297. doi: 10.1017/S0022112089002302.

Maddux, T. B., Cowen, E.A. Haller, M.C. and T.P. Stanton. 2006. The Cross-shore sediment transport experiment (CROSSTEX), *Proceedings of the 30th Int.Conf. on Coastal Engineering,* San Diego, USA: 2547-2558.

Ribberink, J.S. and A.A. Al-Salem. 1994. Sediment transport in oscillatory boundary layers in cases of rippled beds and sheet flow, *Journ. of Geoph. Res.,* Vol. 99, No. C6, 12707-12727, June.

Roelvink, J.A. and A. Reniers. 1995. LIP 11D Delta Flume Experiments - Data report. *W. D. Hydraulics.* Delft, The Netherlands: 124 pp.

Van der A, D. A., Ribberink, J.S., van der Werf, J.J., O'Donoghue, T., Buijsrogge, R.H. and W.M. Kranenburg. 2013. Practical sand transport formula for non-breaking waves and currents, *Coastal Engineering* 76: 26-42, doi: 10.1016/j.coastaleng.2013.01.007.

Van der Zanden, J., Alsina, J.M., Cáceres, I., Buijsrogge, R.H. and J.S. Ribberink. 2013. New CCM technique for sheet-flow measurements and its first application in swasha-zone experiments, *Short Course/Conference on Applied Coastal Research,* Lisbon, Portugal, 10 pp.

Van Rijn, L. C. 2007. Unified view of sediment transport by currents and waves. I: Initiation of motion, bed roughness, and bed-load transport. *Journal of Hydraulic Engineering - ASCE* 133(6): 649-667, doi: 10.1061/(Asce)0733-9429(2007)133:6(649).

Van Rijn, L.C. 2009. Prediction of dune erosion due to storms , *Coastal Engineering* 56(4): 441-457. doi: 10.1016/j.coastaleng.2008.10.006.

Van Rijn, L.C., Ribberink, J.S., Van der Werf, J.J. and D.J.R. Walstra. 2013. Coastal sediment dynamics: recent advances and future research needs, *Journal of Hydraulic Research* Vol. 51, No. 5 (2013), pp. 475–493, doi: 10.1080/00221686.2013.849297.

Vincent, C.E. and D.M. Hanes. 2002. The accumulation and decay of nearbed suspended sand concentration due to waves and wave groups. *Cont. Shelf Res.*, 22, 1987 - 2000.